

Measurement of the Shear Strength of a Charge Density Wave

K. O'Neill, K. Cicak, and R. E. Thorne

Laboratory of Atomic and Solid State Physics, Clark Hall, Cornell University, Ithaca, New York 14853-2501, USA

(Received 3 December 2003; published 6 August 2004)

We have explored the shear plasticity of charge density waves (CDWs) in NbSe_3 samples with cross sections having a single microfabricated thickness step. Shear stresses along the step result from thickness-dependent CDW pinning. For small thickness differences the CDW depins elastically at the volume average depinning field. For large thickness differences the thicker, more weakly pinned side depins first via plastic shear, and shear plasticity contributes substantial dissipation well above the depinning field. A simple model describes the qualitative features of our data and yields a value for the CDW's shear strength of approximately $9.5 \times 10^3 \text{ Nm}^{-2}$. This value is orders of magnitude smaller than the CDW's longitudinal modulus but much larger than corresponding values for flux line lattices, and in part explains the relative coherence of the CDW response.

DOI: 10.1103/PhysRevLett.93.066601

PACS numbers: 72.15.Nj, 71.45.Lr, 73.23.-b, 74.25.Qt

The elastic and plastic properties of driven periodic media including charge/spin density waves (CDWs/SDWs) [1], flux line lattices in type-II superconductors [2–4], and Wigner crystals [5] are central to understanding their rich dynamics and phase behavior. Impurities, dislocations, and other disorder pin the periodic medium in each case so that a minimum or threshold force must be applied to produce collective motion. Shear moduli are especially important because they determine the extent of shear plasticity. In experiments on moving flux line lattices, shear plasticity dominates so that the coherent oscillations at the washboard frequency ν_λ expected in a purely elastic system are replaced by an incoherent response with large $\frac{1}{f}$ -like noise [6], and vanishing of the shear modulus leads to liquidlike motion.

Shear plasticity also plays an important role in charge- and spin-density wave motion, rounding the depinning transition, broadening the spectral width of the coherent oscillations, and smearing out velocity steps caused by mode locking to an applied ac drive. Experiments show that this shear primarily results from meso/macroscopic sample inhomogeneities [7]; rare homogeneous samples of the CDW conductor NbSe_3 show highly coherent washboard oscillations and complete harmonic and subharmonic mode locking [8], suggesting that the intrinsic CDW response is nearly elastic.

Here we show that crystals with microfabricated steps running along the direction of CDW conduction show a nonmonotonic variation of their depinning force with the size of the step, due to shear along the step. A simple model reproduces this variation and allows us to determine the CDW's shear strength to be $9.5 \times 10^3 \text{ Nm}^{-2}$. This value is more than 3 orders of magnitude smaller than the shear elastic modulus [9] and 2 orders of magnitude smaller than the contribution of the pinned CDW to the shear modulus of the crystal [10]. It is much larger than for flux line lattices, which explains in part the relative coherence of the CDW response.

NbSe_3 and related quasi-one-dimensional CDW materials grow as long thin ribbons. Shear usually results from steps in crystal thickness associated with small-angle grain boundaries that run along the ribbon (**b**) axis, which corresponds to the direction of CDW motion. Because typical crystal thicknesses are smaller than the CDW's bulk phase correlation length in the thickness (**a***) direction ($\sim 2 \mu\text{m}$ in undoped crystals), the depinning field varies inversely with crystal thickness $E_T \propto \frac{1}{t}$ [11,12]. As a result, thicker regions of the crystal cross section have smaller depinning fields than thinner regions and tend to shear away from them, as illustrated in, e.g., Figures 3 and 4 of Li *et al.* [13].

Detailed information about shear can be obtained by measuring the CDW response versus step height in samples with a single well-defined step, shown in Fig. 1. The CDWs in rectangular regions 1 and 2 of thickness t_1 and t_2 have depinning fields E_{T1} and E_{T2} . They interact via a shear force F_{shear} along the direction

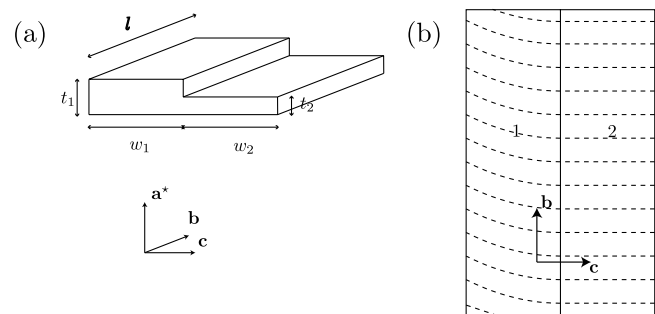


FIG. 1. CDW shear in NbSe_3 . (a) A NbSe_3 single crystal with a step running along its length. Since the pinning strength varies inversely with thickness, the CDW in the thicker part one is more weakly pinned than in the thinner part two. (b) When an electric field greater than the depinning field of part one is applied, the CDW in part one moves relative to part two, producing shear strains.

of CDW motion at the interface between them. This force acts to retard motion of the thicker, more weakly pinned region 1 and assist motion of the thinner, more strongly pinned region 2.

If no slip occurs at the boundary (the static friction regime), then elastic coupling causes regions 1 and 2 to depin at a common field E_T given by

$$E_{T,el} = \frac{E_{T1}t_1w_1 + E_{T2}t_2w_2}{t_1w_1 + t_2w_2}, \quad (1)$$

where w_1 and w_2 are the widths of regions 1 and 2, respectively. In thin crystals where $E_T \propto \frac{1}{l}$ and assuming $w_1 = w_2$, Eq. (1) reduces to $E_{T,el} = 2E_{T1}/(1 + \frac{t_2}{t_1})$.

The frictional force F_{shear} has a maximum static value F_{max} , beyond which plastic slip occurs along the interface. The thick region 1 shears and slides relative to the thin region 2 at a field

$$E_{T,pl} = E_{T1} + \frac{F_{\text{max}}}{Q_1}, \quad (2)$$

where $Q_1 = en_cw_1t_1l$ is the total CDW charge in region 1 which couples to the electric field. The maximum shear force should be proportional to the area of the interface between the two regions, and thus to t_2 . With t_1 fixed, Eq. (2) becomes

$$E_{T,pl} = E_{T1} + \frac{\sigma_s}{en_cw_1} \frac{t_2}{t_1}, \quad (3)$$

where σ_s is the plastic shear strength.

To study CDW shear, a NbSe₃ crystal with a nearly rectangular cross section is selected and placed on a substrate patterned with an array of nonperturbing gold electrical probes, each 2 μm wide in the direction of CDW motion. At least 1 μm of UV-5 resist is spun onto the crystal and substrate and then cured at 130°C, the highest temperature to which the crystal is exposed during processing. The resist is patterned using a Cambridge-LEICA E-beam system 10.5. After developing, the pattern is etched into the sample using a CF₄ dry plasma etch. The etch depth and spatial consistency can be monitored using the resistance per unit length for each probe pair along the sample. The average thickness is then calculated from the optically measured crystal width and NbSe₃'s room temperature resistivity of 1.86 $\Omega\mu\text{m}$ [12]. More details on the fabrication process are found in [14].

We explored two different sample designs. The first, shown in Fig. 2(a) and 2(b), has three distinct cross sections: an as-grown rectangular segment at one end with thickness t_1 , an etched rectangular segment at the other end with thickness t_2 , and a middle segment with a step running along **b** separating unetched and etched regions of thickness t_1 and t_2 , respectively.

The second sample design, shown in Fig. 2(c) and 2(d), is etched to produce a thickness step along its entire

length. This eliminates current density changes and contributions to E_T from longitudinal phase slip [15] present in the first design, and thus yields more precise measurements of shear effects on E_T . The NbSe₃ crystal used had two small steps. A portion of the crystal width containing the steps was thinned by repeated etching through the same resist mask, as shown in Fig. 2(c), and transport measurements were performed after each etch. This yielded E_T as a function of the thickness ratio $\frac{t_2}{t_1}$. This process was then repeated using the remaining, initially step-free part of the crystal, as shown in Fig. 2(d). Data for two samples, A and B, fabricated using the first and second process, respectively, are described here. Measurements were performed at $T = 120$ K where longitudinal phase slip contributions to E_T are smallest. For both samples the thickness was less than the bulk CDW phase-phase correlation length in the **a*** direction so that depinning fields $E_T \propto 1/t$ are expected.

Figures 3(a) and 3(b) show the measured four-probe differential resistance $\frac{dV}{dI}$ versus electric field on Samples A and B, respectively. For Sample A, the unetched region

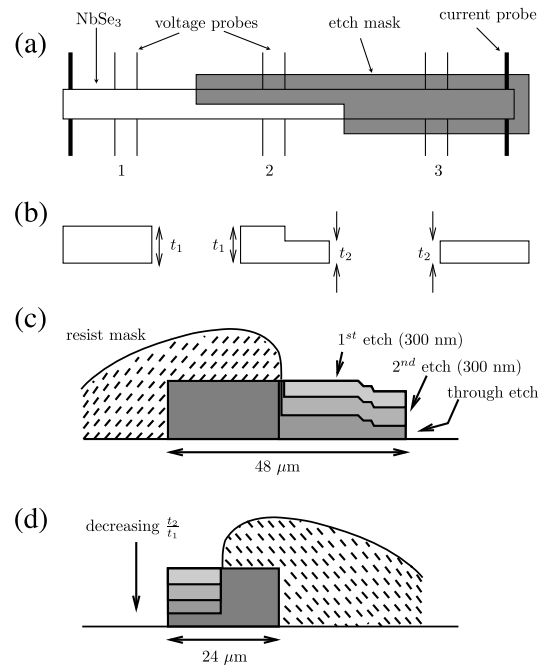


FIG. 2. (a) Sample A. Etching thinned the sample region not covered by the mask, and the resulting crystal cross sections in sample segments 1, 2, and 3 are shown in (b). The sample width was 62 μm , its unetched thickness was $t_1 = 0.52$ μm , and the etched region thickness was $t_2 = 0.26$ μm . (c) and (d) Sample B. The step is etched through a resist mask along the entire sample length. The unetched sample was 48 μm wide and 0.89 μm thick. After the first etch sequence in (c), the entire crystal was reduced to half its original width, and preexisting growth steps removed. A second etch sequence (d) on the rectangular sample produced in (c) yielded the most accurate measurements of depinning field versus $\frac{t_2}{t_1}$.

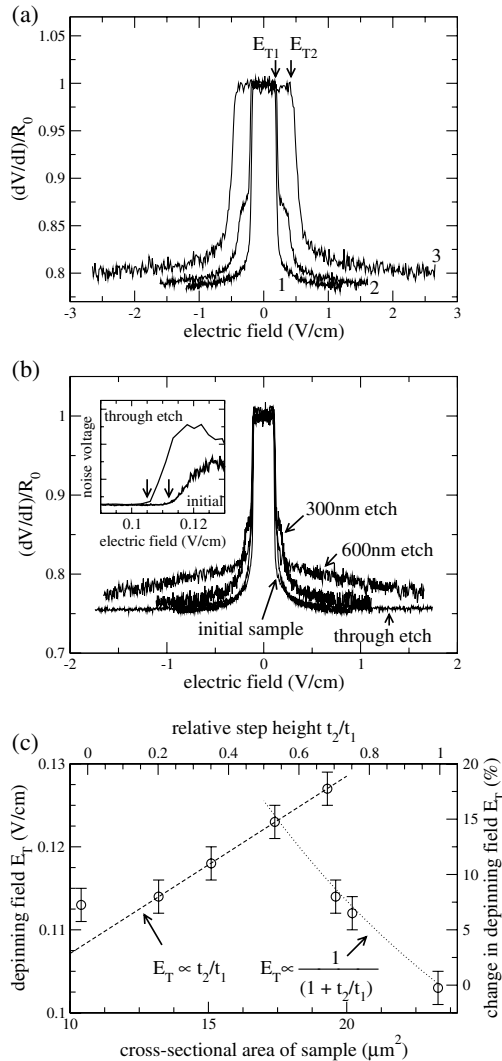


FIG. 3. (a) Normalized $\frac{dV}{dI}$ versus electric field at $T = 120$ K for sample A. Curves 1, 2, and 3 were measured between voltage probes on segments 1, 2, and 3 in Fig. 2(a), respectively. $\frac{dV}{dI}$ drops abruptly from the low-field single particle resistance at the collective depinning field E_T . (b) Normalized $\frac{dV}{dI}$ and versus electric field at $T = 120$ K for sample B, acquired during the first etch sequence in Fig. 2(c). The inset shows the noise amplitude, measured in a 4 Hz bandwidth around 20 Hz, that abruptly increases at E_T . (c) Depinning field E_T (from noise measurements) versus thickness ratio t_2/t_1 and cross-sectional area, obtained for Sample B during the second etch sequence of Fig. 2(d).

1 and uniformly etched region 3 have depinning fields E_T in the ratio 1:2.4. This roughly matches the thickness ratio 1:2.0 determined from room temperature resistance measurements. Consequently, despite producing a somewhat rougher surface, etching yields roughly the same thickness-dependent E_T as is observed in unetched crystals of different thicknesses [12]. Curve 2 in Fig. 3(a) for the stepped segment 2 shows two separate depinnings for the etched and unetched portions of the crystal cross

section. The smaller depinning field of the unetched portion is increased only slightly from that of the unetched and step-free segment 1, suggesting that it shears from the etched portion. The larger depinning field of the thin, etched portion is lower than that of the unstepped etched segment 3, indicating that shear forces exerted by the depinned CDW in the thick portion assist depinning in the thin portion.

For Sample B, the normalized resistivities versus field in Fig. 3(b) for the initial, unetched sample and for the through-etched sample are nearly identical and show a large, abrupt drop at E_T , indicating excellent sample quality and that sidewall roughness induced by etching is unimportant. In contrast, for partial etching the differential resistance well above E_T is significantly larger than for the unetched or through-etched sample. The differential conductance associated with CDW motion at $E = 16E_T$ is 9% smaller for a 600 nm etch depth ($t_2/t_1 = 0.33$) than for the through-etched crystal. This indicates that shear friction—in the form of shear-induced CDW phase vortex/dislocation “turbulence”—along the step strongly affects CDW dynamics.

To accurately determine how the depinning field of Sample B varies with etched thickness (t_2/t_1), both the low-frequency noise amplitude and the differential resistance were measured versus electric field, as shown in Fig. 3. The noise amplitude increases by orders of magnitude when the CDW or a portion of it depins [16] and provides the most sensitive probe of E_T . The cleanest data were obtained for the second etch sequence of Fig. 2(d), starting with the rectangular cross section produced in 2(c). To simplify interpretation, the widths of the etched and unetched portions were chosen to be nearly identical and equal to $12 \mu\text{m}$.

Figure 3(c) shows the depinning field E_T versus both sample cross-sectional area and thickness ratio $\frac{t_2}{t_1}$. Although there is some scatter, the data clearly show two distinct regimes. For $\frac{t_2}{t_1}$ close to 1 (small steps), E_T increases with decreasing $\frac{t_2}{t_1}$. For $\frac{t_2}{t_1}$ close to 0 (large steps), E_T increases with increasing $\frac{t_2}{t_1}$. This general behavior is consistent with the simple model of Eqs. (1)–(3). For large etch thicknesses $\frac{t_2}{t_1} \lesssim 1$, the shear stress at the boundary between etched and unetched regions is small. $\frac{dV}{dI}$ drops sharply and smoothly, indicating that the entire sample volume depins at a unique E_T , determined by the volume average of E_{T1} and E_{T2} given by Eq. (1). As the etched thickness and $\frac{t_2}{t_1}$ decrease, the shear stress σ_s eventually is sufficient to cause shear slip along the boundary. In this case, $\frac{dV}{dI}$ shows two successive “drops” corresponding to depinning of the unetched (thick) and etched (thin) regions, respectively. The thick region’s depinning field E_T is the sum of the pinning force $\propto E_{T1}$ in that region and the maximum retarding shear force exerted across the area of contact between the CDWs. This is determined by

the maximum shear stress $\sigma_{s,\max}$ (force/area) times the contact area $\propto t_2$ and is given by Eq. (2).

The dotted and dashed lines in Fig. 3(c) are fits to Eqs. (1) and (2) in the elastic and plastic regimes, respectively. The overall qualitative agreement is remarkable given the simplicity of our model. The elastic regime fit has no adjustable parameters, since $E_T(t)$ for our undoped NbSe₃ crystals has been determined in independent measurements [12], and is in good quantitative agreement as well. The CDW's elastic shear stress along the boundary grows as t_2/t_1 becomes smaller. From the location of the crossover between the elastic and plastic regimes we can estimate the CDW's maximum elastic shear stress from Eq. (3) as $\sigma_s = \frac{en_c w_1}{2} \frac{t_1}{t_2} [E_T(\frac{t_2}{t_1}) - E_{T1}]$. Using the known cross-section dimensions w_1 , t_1 , and t_2 , a condensate density $n_c = 1.9 \times 10^{21} \text{ cm}^{-3}$ and the value of E_T from the elastic fit at $t_2/t_1 = 0.66$ yields $\sigma_{\max,\text{el}} = 6.6 \times 10^3 \text{ Nm}^{-2}$. The plastic fit (dashed line) in Fig. 3(c) is given by $E_T(\frac{t_2}{t_1}) - E_T(0) \approx 0.026 \frac{t_2}{t_1}$ (in Vcm^{-1}). From this fit we obtain the plastic shear strength σ_s at the interface between the thick and thin portions of the sample of $\sigma_s \approx 9.5 \times 10^3 \text{ Nm}^{-2}$, in rough agreement with the maximum elastic shear strength. These estimates do not account for the effects of nonuniform stresses along the interface due to the L-shaped cross section.

A rough lower bound for the CDW's shear modulus C may be estimated from the ratio of the maximum elastic shear stress to the CDW shear strain when adjacent chains are $\frac{\pi}{2}$ out of phase. This gives the relation $\sigma_s \leq \frac{1}{4} \frac{\lambda_c}{d} C$, where λ_c is the CDW wavelength and d is the distance between adjacent chains [17]. This gives $C \geq 2.1 \times 10^4 \text{ Nm}^{-2}$, more than 3 orders of magnitude smaller than NbSe₃'s elastic shear modulus $\sim 3 \times 10^7 \text{ Nm}^{-2}$ determined by scaling its measured longitudinal modulus $\sim 2.6 \times 10^8 \text{ Nm}^{-2}$ [9] by the measured ratio ~ 10 of the longitudinal and transverse CDW correlation lengths. As in ordinary crystals and flux line lattices, the measured stress is likely reduced from its theoretical value by crystal and CDW defects.

The elastic moduli of flux line lattices depend on magnetic field. The shear modulus c_{66} increases roughly linearly at small fields, reaching a maximum at intermediate fields before dropping to zero at high fields. In Nb₃Ge, the maximum value is $\sim 10 \text{ Nm}^{-2}$ at $\frac{B}{B_{c2}} \sim 0.3$ [18]. Measurements on vortices in nm-scale, weakly pinned Nb₃Ge channels in a strongly pinned background [18] yield a maximum plastic shear strength at $\frac{I}{I_c} = 0.6$ and $\frac{B}{B_{c2}} \sim 0.4$ of $\sim 0.4 \text{ Nm}^{-2}$. These shear moduli and shear strength values are roughly 6 and 4 orders of magnitude smaller, respectively, than the corresponding CDW values, consistent with the much more nearly elastic collective response of CDWs. The character of the bulk collective response depends on the ratio of the elastic

strength to the bulk pinning strength, which is reflected in the ratio of the correlation length to the lattice periodicity. In CDW systems this ratio is typically 10^3 to 10^4 , 2 to 3 orders of magnitude larger than is typical in flux line lattices.

In conclusion, we have observed a crossover from elastic to plastic behavior in the depinning of charge-density waves in crystals with artificially produced cross-section steps. From this behavior we have determined the shear strength of the T_{P1} CDW in NbSe₃. This measurement provides a basis for understanding shear plasticity in CDW systems and its relation to plasticity observed in other driven disordered media.

We thank Rut Besseling for fruitful discussions. This work was supported by the National Science Foundation (NSF) (Grants No. DMR 0101574 and No. INT 9812326). K. O'N. was supported by the U.S. Department of Education. Nanofabrication work was performed at the Cornell Nano-Scale Science & Technology Facility, supported by the NSF (Grant No. ECS-9731293), its users, and its industrial affiliates.

-
- [1] D. Feinberg and J. Friedel, in *Low-Dimensional Electronic Properties of Molybdenum Bronzes and Oxides*, edited by C. Schlenker (Kluwer Academic, Dordrecht, 1989), p. 407.
 - [2] G. Blatter *et al.*, Rev. Mod. Phys. **66**, 1125 (1994).
 - [3] M.C. Marchetti and D.R. Nelson, Physica C (Amsterdam) **330C**, 105 (2000); P. Benetatos and M.C. Marchetti, Phys. Rev. B **65**, 134517 (2002).
 - [4] S. Yoon *et al.*, Science **255**, 165 (1992); M. Marchevsky *et al.*, Phys. Rev. B **57**, 6061 (1998).
 - [5] E.Y. Andrei *et al.*, Phys. Rev. Lett. **60**, 2765 (1988).
 - [6] J.R. Clem, Phys. Rep. **75**, 1 (1981).
 - [7] M.P. Maher *et al.*, Phys. Rev. B **43**, 9968 (1991).
 - [8] R.E. Thorne *et al.*, Phys. Rev. B **35**, 6348 (1987).
 - [9] D. DiCarlo *et al.*, Phys. Rev. Lett. **70**, 845 (1993); T.L. Adelman *et al.*, Phys. Rev. B **52**, R5483 (1995).
 - [10] X.-D. Xiang and J.W. Brill, Phys. Rev. B **39**, 1290 (1989).
 - [11] P.J. Yetman and J.C. Gill, Solid State Commun. **62**, 201 (1987).
 - [12] J. McCarten *et al.*, Phys. Rev. B **46**, 4456 (1992).
 - [13] Y. Li *et al.*, Phys. Rev. Lett. **83**, 3514 (1999). X-ray images indicate that shear strains at thickness steps are much larger than those associated with pinning and contact effects at the temperatures studied here.
 - [14] K. O'Neill *et al.*, J. Phys. IV (France) **12**, 185 (2002).
 - [15] J.C. Gill, J. Phys. C **19**, 6589 (1986); M.P. Maher *et al.*, Phys. Rev. B **52**, 13850 (1995).
 - [16] R.M. Fleming and C.C. Grimes, Phys. Rev. Lett. **42**, 1423 (1979).
 - [17] S. van Smaalen *et al.*, Phys. Rev. B **45**, 3103 (1992).
 - [18] A. Pruyboom *et al.*, Phys. Rev. Lett. **60**, 1430 (1988); R. Besseling *et al.*, Europhys. Lett. **62**, 419 (2003).